

Article

Regionally-Coherent Embayment Rotation: Behavioural Response to Bi-Directional Waves and Atmospheric Forcing

Mark Wiggins *, Tim Scott, Gerd Masselink, Paul Russell and Nieves G. Valiente

Coastal Processes Research Group, University of Plymouth, Devon PL4 8AA, UK; timothy.Scott@plymouth.ac.uk (T.S.); Gerd.masselink@plymouth.ac.uk (G.M.); P.Russell@plymouth.ac.uk (P.R.); Nieves.garciavaliente@plymouth.ac.uk (N.G.V.)

* Correspondence: mark.wiggins@plymouth.ac.uk; Tel.: +44-7962263581

Received: 30 March 2019; Accepted: 16 April 2019; Published: 23 April 2019



Abstract: Bi-directional wave climates often drive beach rotation, increasing erosional risk at semi-sheltered locations. Identification of rotation and forcing mechanisms is vital to future coastal defence. In this study, regional investigation of modelled wave data revealed strong bi-directionality between dominant south-westerly and sub-dominant easterly waves for 14 offshore locations along the length of the south coast of England, U.K. South-westerly wave power was well correlated to positive phases of the West Europe Pressure Anomaly (WEPA), whilst easterly wave power was well correlated with negative phases of the North Atlantic Oscillation (NAO). Additionally, decadal records of beach morphological change and associated wave forcing, were investigated for 22 coastal sites across the same region. Significant rotational behaviour was identified at 11 sites, leading to the creation of a rotation index. Beach rotation was attributed to shoreline angle, with the strongest rotation occurring at south-east-facing beaches, with high obliquity to dominant south-westerly waves. The beach rotation index was well correlated with the normalized balance of wave power from opposing south-westerly and easterly directions. Direct correlations between beach rotation and WEPA at two sites showed that future forecasts of atmospheric indices may allow prediction of rotational beach state, at seasonal scales.

Keywords: beach rotation; bi-directional waves; NAO; WEPA; erosion; storm; winter; atmospheric oscillations; climate indices

1. Introduction

Coastal rotation is observed worldwide at many semi-sheltered, often embayed locations, particularly where wave climates are bi-directional [1]. Alongshore transport of sediment as a result of opposing wave directions, especially following storm events, can lead to an imbalance of erosion and accretion at embayment extremities. This can leave coastal communities and infrastructure vulnerable to damage from future storm events [2,3], seasonal changes in wave climate [4] and atmospheric changes over decadal timescales [5]. To mitigate these impacts, identification of rotational beach behaviour, its drivers and controls is required for planning and management of the coastal zone, given future predictions of sea level rise [6], increased storminess [7] and coastal squeeze [8].

Many site-specific studies of beach rotation [3,9–12] have identified variability in the local bi-directional wave climate as a key control of the beach morphological state. Wiggins et al. [4] identified that winter changes in beach profile volume change, at opposing ends of a single semi-sheltered gravel embayment (Slapton Sands, U.K.; facing south-east up the English Channel), are well correlated to the relative balance of the normalized contributions of winter wave power from opposing directions.

This power balance, and the individual contributions of directional wave power, were also shown to be significantly correlated with both the North Atlantic Oscillation (NAO) and the newly-devised West Europe Pressure Anomaly (WEPA) [13]. The study by Wiggins et al. [4] did not directly compare beach rotation with atmospheric indices; however, several authors have identified direct links between changes in beach morphology and different phases of climatic oscillations, including the El Niño/La Niña Southern Oscillation (ENSO) [14–16], NAO [12,17], and WEPA [18,19].

This study firstly assesses whether, across a regional domain, wave climates exhibit bi-directional characteristics and whether similar correlations with atmospheric indices (NAO and WEPA) are observed for the whole south coast of England, U.K. Secondly, we assess whether beach rotational behaviour can be identified at a multitude of different sites, by evaluating the decadal morphological response of 22 different coastal locations. Where rotation can be identified, we assess to what extent the wave climate balance and shoreline orientation are controlling factors. Lastly, we investigate whether climate indices can be directly correlated to beach rotation. If wave climate and beach rotation are regionally coherent beyond a few single case studies and well correlated to climate indices, then improved “season ahead” forecasts of NAO [20,21] and WEPA [22] may lead to direct predictions of beach rotation and subsequent coastal vulnerability at regional scales.

2. Materials and Methods

2.1. Wave Data

For the length of the south coast of England, wave data were obtained for 14 offshore node locations (Figure 1), comprised of 3-hourly hindcast Wave Watch III model data (obtained from the U.K. Meteorological Office), spanning the years from 1980–2016. Offshore, significant wave height, mean wave energy period and peak direction were utilized in assessing directional wave power variability in wave climate across all node locations. Wave power (P) is calculated at each model node using:

$$P = 1/16 \rho g H_s^2 C_g \tag{1}$$

where ρ is water density, g is acceleration due to gravity, H_s is significant wave height and C_g is wave celerity calculated with linear wave theory using wave energy period (T_e) and local water depth (h).

Additional short-term records (up to 13 years, 2003–2016) of inshore measured wave conditions were obtained from a wave buoy network (obtained from the Channel Coastal Observatory), for a limited number of locations along the length of the coastline. These were used to compare the inshore wave climate to the modelled conditions offshore.

2.2. Wave Power Directionality Index

At all locations, an assessment of the primary (P_{Dir1}) and secondary (P_{Dir2}) wave directional modes was made. Wave power was then subdivided into contributions coming from these two directions, and an index of the relative balance of the two was computed, and henceforth named the Wave power Directionality Index (WDI), using the equation:

$$WDI = \frac{(P_{Dir1} - P_{Dir2}) - \overline{(P_{Dir1} - P_{Dir2})}}{\sigma(P_{Dir1} - P_{Dir2})}, \tag{2}$$

where $(P_{Dir1} - P_{Dir2})$ is the residual wave power between the first and second directional modes, $\overline{P_{Dir1} - P_{Dir2}}$ is the long-term mean and $\sigma(P_{Dir1} - P_{Dir2})$ is the long-term standard deviation of that difference. High positive values of WDI indicate that the primary directional mode is more prevalent than the long-term average, whereas high negative values indicate that the wave climate has a higher proportion of the secondary directional mode than average.

The wave power for each directional mode, as well as the WDI was calculated for the period spanning December, January, February and March (DJFM), to give a winter average of each variable

over the 36-year period at each node location. These wave characteristics were later correlated with atmospheric controls and morphological change, described next.

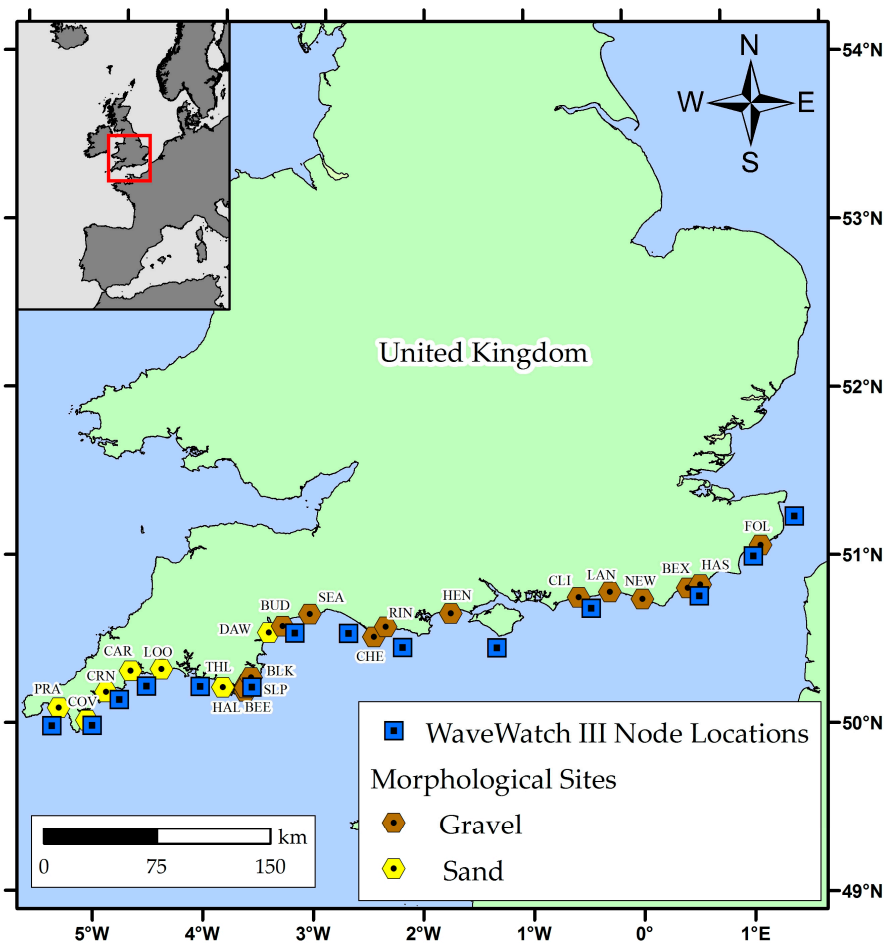


Figure 1. Wave Watch III model wave nodes (squares) and morphological study site locations (hexagons) along the south coast of England, U.K. Site location names are abbreviated here and used when presenting further results. An index of site locations, morphological parameters and survey schedules is located in Appendix A, Tables A1 and A2.

2.3. Morphological Data

Extensive morphological datasets of inter-tidal, cross-shore beach profiles were collated from a multitude of coastal sites, along the length of the south coast of England (Figure 1; further site information and survey schedules are provided in Appendix A, Tables A1 and A2). Unfortunately, quantitative records of beach grain sizes were not available across the full extent of the surveyed beaches; however, a qualitative distinction between gravel ($\varphi < -1$ or $D_{50} > 2$ mm) or sand ($\varphi > -1$ or $D_{50} < 2$ mm) was made for each site. Beach surveys were conducted during Mean Low Water Spring (MLWS) tides, using Real-Time Kinematic Global Positioning Systems (RTK-GPS), providing vertical accuracy of <30 mm. The frequency of surveys varied within and between site records, ranging from 4-monthly to yearly, with records spanning from 10–15 years. For each survey date, cross-shore beach volumes were calculated at equally-spaced profiles (between 150 and 250 m depending on location). Individual profile volumes at adjacent locations were averaged for opposing ends of beach extents (Figure 2), to produce a representative mean volume for the eastern (northern) and western (southern) sections.

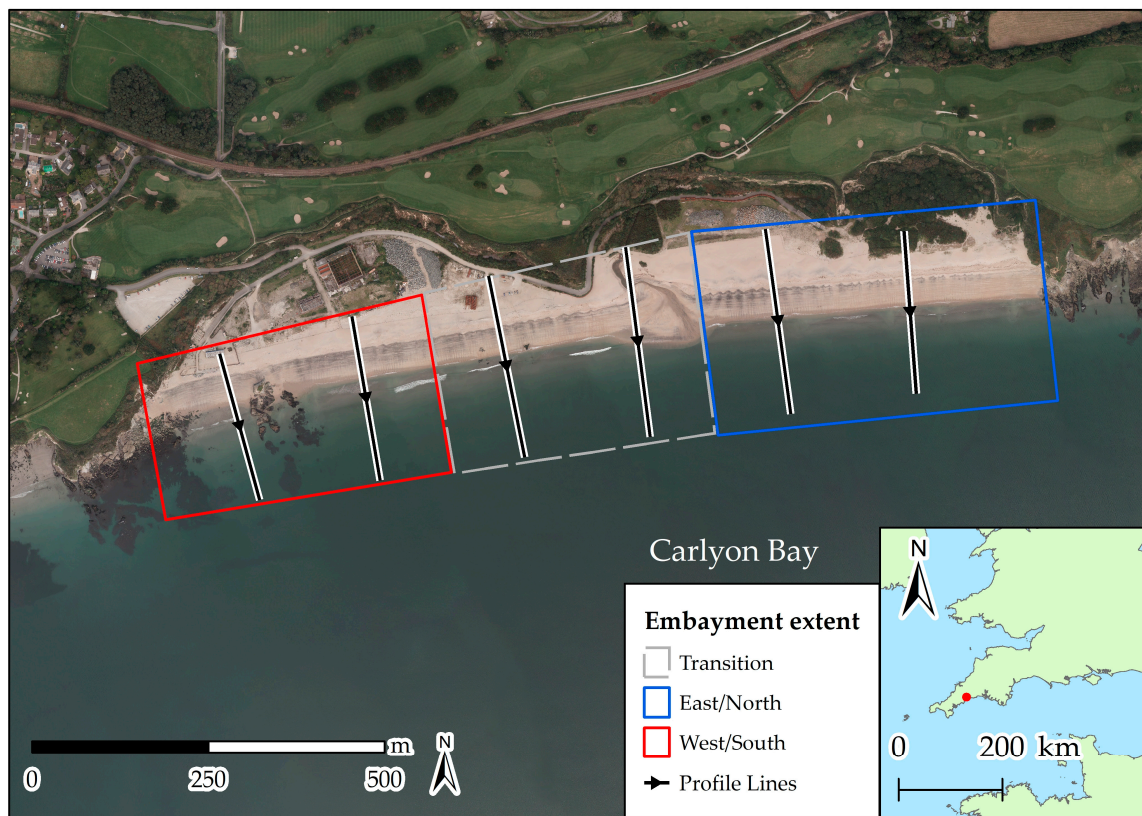


Figure 2. Example of beach morphology extents for Carlyon Bay (CAR). The black arrowed lines represent measured profile locations. Beach volumes for the east (west) or north (south) extents are averaged along the length of the blue (red) box. The grey dashed box represents the central nodal point of the embayment, and as such, the beach volume for this region is omitted.

Normalizing the resultant average volumes by their mean and range produced a time series of values ranging between 0 (lowest volume, most eroded) and 1 (highest volume, most accreted). Volume change (dV_i) at opposing ends was then calculated for each time-step (V_i) by subtracting the previous normalized volume (V_{i-1}) such that:

$$dV_i = V_i - V_{i-1} \tag{3}$$

2.4. Beach Morphological Response

Assessment of the behaviour for each coastal location was then conducted by calculating a Beach Morphological Response (BMR), defined as the correlation coefficient of the linear regression of western (southern) volume change dV_i (west), against the eastern (southern) volume change dV_i (east). Where the correlation and hence BMR values were positive, both ends of the beach were responding together, suggesting that the behavioural response was cross-shore dominated. Conversely, at locations where values were negative, the two ends of the beach were responding out of phase, with one end gaining volume, whilst the other losing, suggesting a longshore transport of beach material, and hence rotational response. An example of this regression is shown for Carlyon Bay (CAR) in Figure 3a,b, showing the two beach ends responding out of phase.

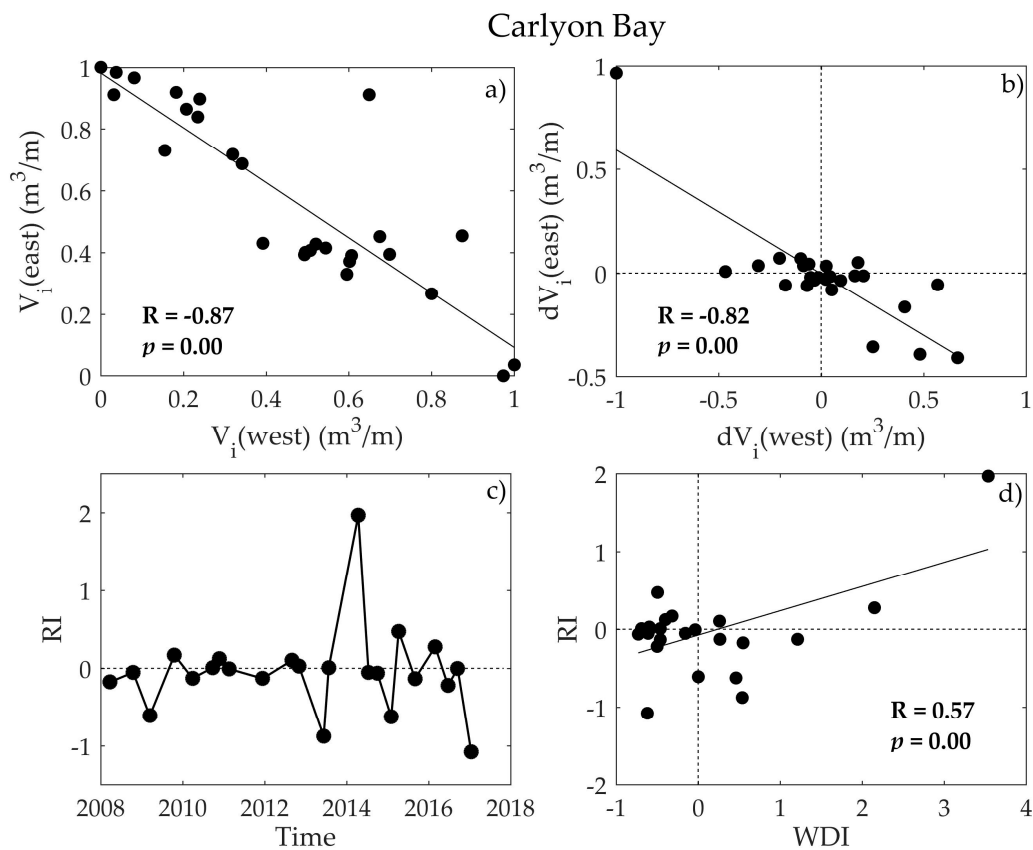


Figure 3. Example of the morphological workflow and parameters for the embayed sandy beach of Carlyon Bay, Cornwall, U.K.: (a) Linear regression of the normalized beach volumes at the western and eastern ends of the beach. (b) Linear regression of the normalized volume change of the same western and eastern beach ends. (c) Time series of the Rotation Index (RI) for the duration of the survey record. (d) Linear regression of the Wave power Directionality Index (WDI) against the RI, highlighting the beach rotational response to increased dominance of one wave direction over another.

2.5. Rotation Index

To quantify the strength and direction of the beach rotational response for each site, at each time step, a Rotation Index (RI) was calculated by subtracting the western (southern) volume change from the eastern (northern) volume change such that:

$$RI = dV_i(\text{east}) - dV_i(\text{west}), \tag{4}$$

When RI was highly positive, the beach response exhibited a strong clockwise rotation, whereas high negative values indicated an anti-clockwise rotation. Where values of RI tended towards zero, both ends were responding in phase, and beach rotation was minimal. The time series of the RI for Carlyon Bay is shown in Figure 3c, highlighting the phases of clockwise and anti-clockwise rotation. The WDI and RI for each site were also correlated against each other, as seen in Figure 3d, with results for the remaining sites presented later in Section 3.2.

2.6. Atmospheric Indices and Climate Control

In addition to the wave climate and morphological datasets identified above, winter averages of both NAO and WEPA were obtained for the time period of the modelled wave data. Winter averages (DJFM) of NAO [23] and WEPA [13] were derived from station-based differences of sea level pressure.

3. Results

3.1. Wave Climate Spatial Variability

The offshore modelled wave climate was predominantly bi-directional along the length of the south coast (Figure 4). In all locations, the primary wave direction was from the south west (greater than 180° and less than 270°). Secondary modes, where apparent, were from easterly directions (less than 180°).

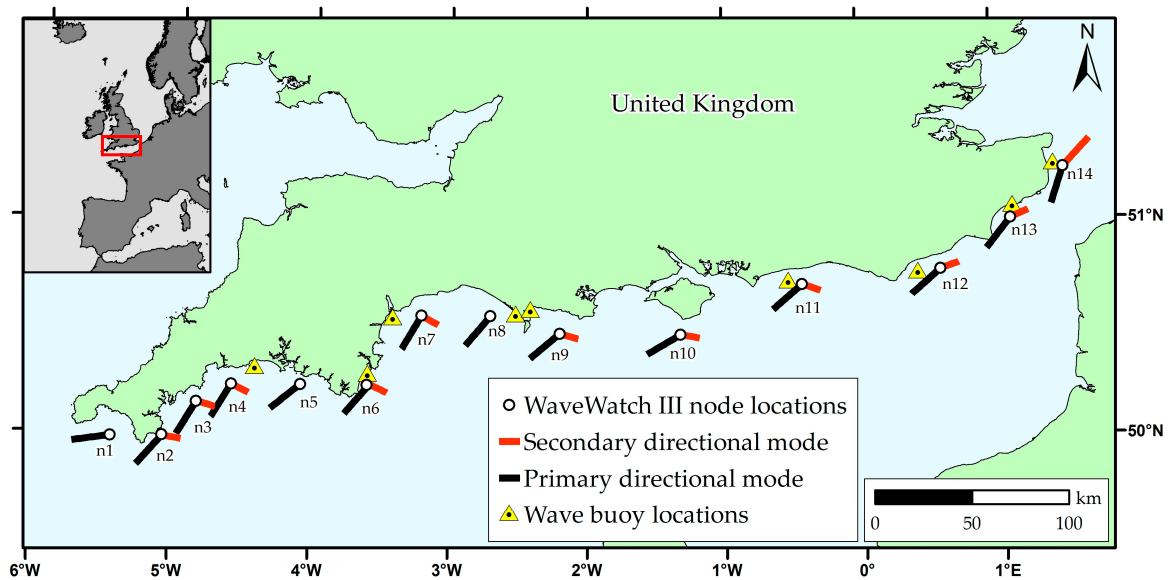


Figure 4. Bi-directional wave climate along the south coast of the English Channel, showing the primary directional mode in black and the second directional mode in red, averaged from a 36-year Wave Watch III modelled record. Inshore wave buoy locations are indicated by yellow triangles.

Despite the bi-directional nature of the wave climate, winter averages (DJFM) of directional wave power across all node locations for the 36-year period showed that south-westerly wave power was greater than easterly wave power (Figure 5a). The imbalance of directional wave power was less pronounced at inshore locations, as the wave characteristics were often modified by coastline orientation, potential shelter, refraction and shoaling due to inshore bathymetry and headlands. In addition to the modelled wave data, measured data from inshore wave buoy locations (Figure 4) were used to calculate the balance of southerly to easterly waves, with results displayed in Figure 5b.

At locations where there was a degree of shelter from south-westerly waves (e.g., buoy locations closest to Nodes 6, 7 and 9), measured inshore total wave power averages were lower than those modelled offshore, and easterly waves contributed a larger percentage to the winter average balance of the two wave directions. For example, over the same time period (2007–2016), the winter averaged contribution of easterly wave power increased from 16% offshore at Node 6 to 39% of the total wave power measured at the closest inshore wave buoy (Start Bay, Devon). Similar increases in easterly wave contributions were seen at Node 7 (15% offshore to 45% inshore) and Node 9 (5% offshore to 28% inshore).

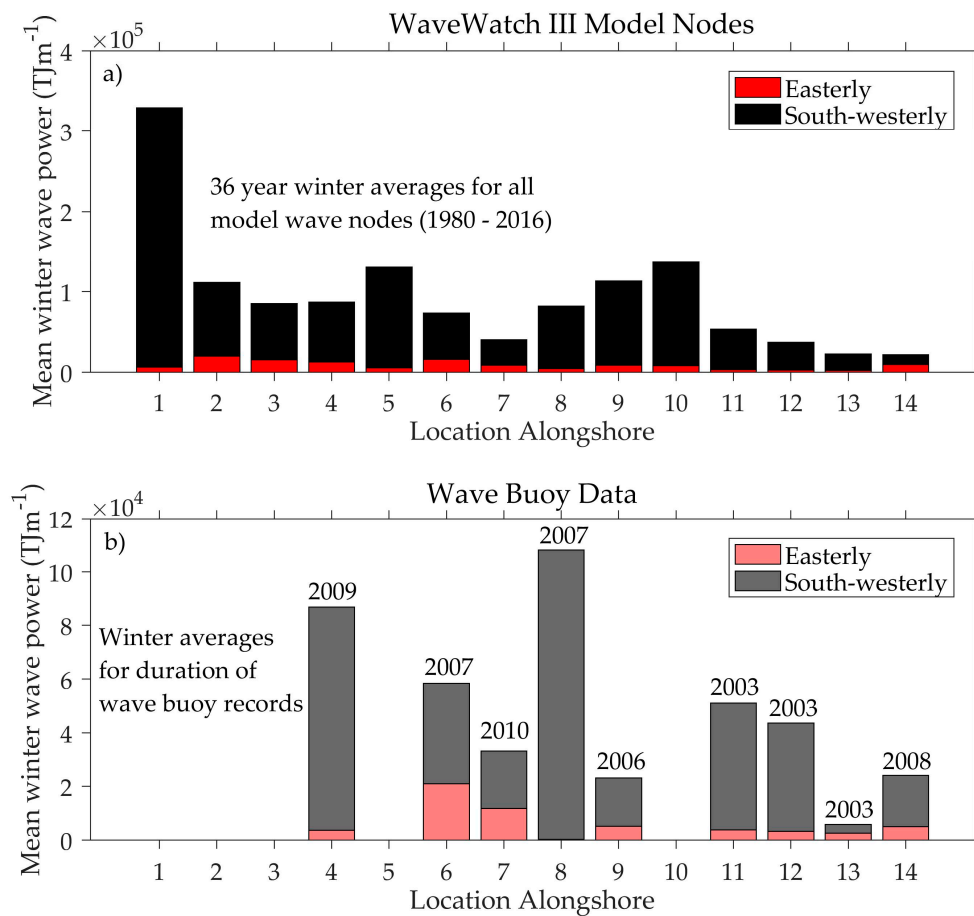


Figure 5. (a) Thirty-six-year long-term averages of winter (DJFM) wave power from both easterly (red) and southerly (black) directions for each offshore Wave Watch III model node, numbered from west to east (for locations, see Figure 4). (b) Average winter (DJFM) wave power from both easterly (red) and southerly (black) directions for inshore wave buoys closest to the respective node location. The year of wave buoy installation is labelled above each bar, and the record period runs from that year until 2016.

Despite the average dominance of south-westerly to easterly waves, at all bi-directional node locations, there was significant inter-annual variability between directional dominance. As a result, calculated values of WDI indicated years where south-westerly or easterly waves were higher than average. An example time series is shown in Figure 6 and highlights the inter-annual variability for Node n6. The majority of winters were dominated by south-westerly wave power (Figure 6a); however, easterly wave power was greater than south-westerly for some winters (e.g., 1985 and 1996). Those high energy easterly winters were reflected in the two greatest negative values of the WDI (Figure 6b). Similarly, winters with the highest values of south-westerly wave power, with little contribution from easterly waves, showed the highest positive values of WDI (i.e., 1990, 1995, 2007 and 2014).

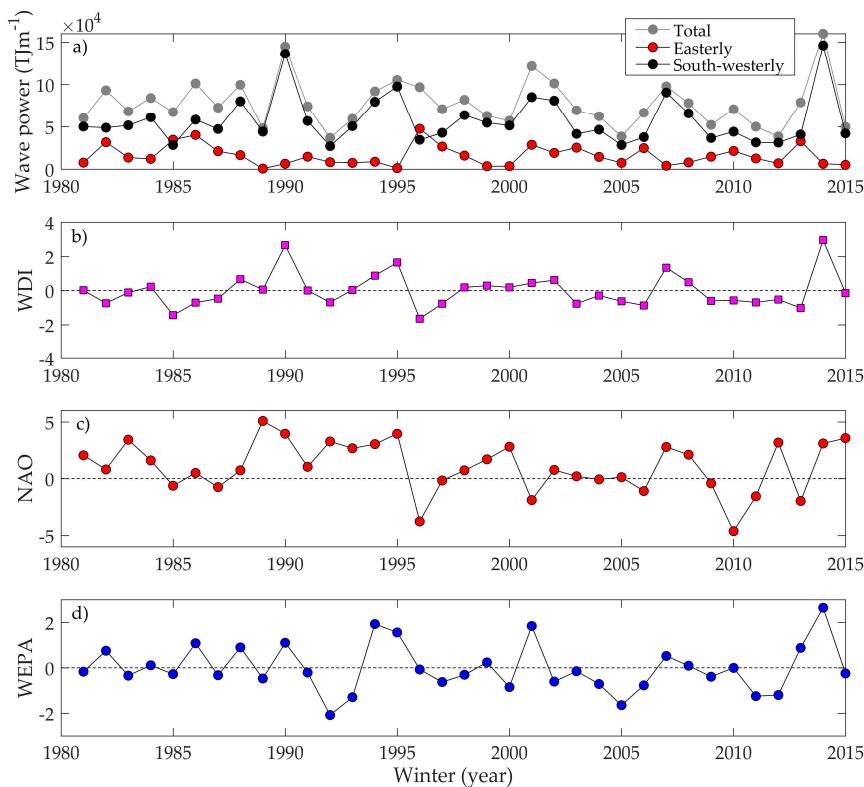


Figure 6. Winter average (DJFM) values of wave climate parameters for the Node n6 located off Start Bay showing: (a) 36 years of winter average total wave power (grey), easterly wave power (red) and south-westerly wave power (black) and (b) winter averages of the WDI showing the balance of south-westerly wave power (positive values) or easterly wave power (negative values) compared to the long-term mean. Winter (DJFM) averages of atmospheric indices showing (c) values of NAO and (d) values of WEPA.

Variations in the winter averaged values of NAO and WEPA (Figure 6c,d) were correlated against wave power contributions and the WDI at this node, and the results are displayed in Table 1. NAO was strongly negatively correlated with easterly wave power, whilst WEPA was strongly positively correlated with south-westerly wave power. The WDI was significantly and positively correlated with both climate indices, suggesting there was some atmospheric control on wave climate.

Table 1. Pearson’s correlation coefficients for atmospheric and wave climate variables, obtained from WaveWatch III model data from Node n6 (see Figure 4 for location). Correlations between winter averages (DJFM) of total wave power, south-westerly wave power, easterly wave power, WDI, NAO and WEPA are presented, with correlations significant at the 95% confidence limit presented in bold.

Variable	Total Power	SW Power	E Power	WDI	NAO	WEPA
Total Power		+0.88	+0.18	+0.68	+0.02	+0.84
SW Power			-0.29	+0.94	+0.37	+0.75
E Power				-0.59	-0.75	+0.12
WDI					+0.58	+0.59
NAO						+0.07
WEPA						

Expanding the analysis across all model nodes and the full spatial extent of the study, wave climate parameters along the length of the English Channel exhibited variable relationships with atmospheric indices (Figure 7). At the eastern end of the English Channel, both total (Figure 7a) and

south-westerly (Figure 7b) wave power were positively and statistically (95% confidence interval) correlated with NAO.

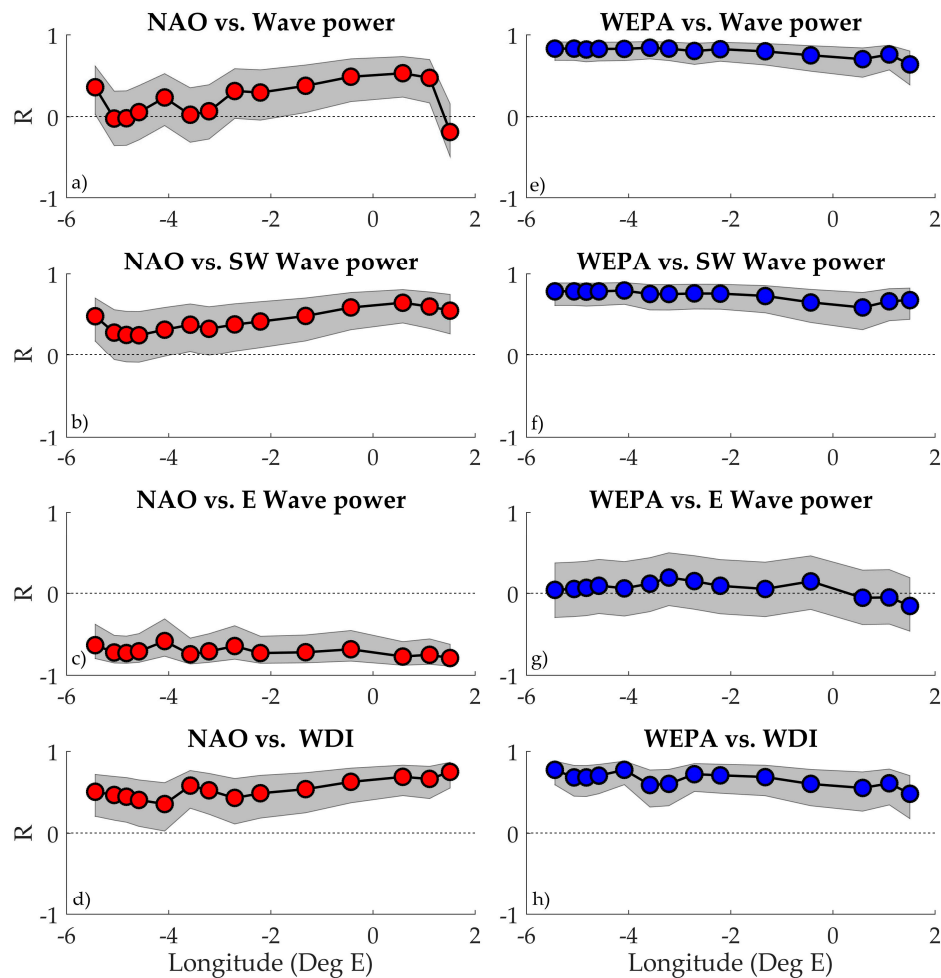


Figure 7. Correlations between winter NAO with (a) total winter wave power, (b) south-westerly wave power (P_{Dir1}), (c) easterly wave power (P_{Dir2}) and (e) WDI. Additional correlations are shown between winter WEPA with (e) total winter wave power, (f) south-westerly wave power (P_{Dir1}), (g) easterly wave power (P_{Dir2}) and (h) WDI. In all plots, 95% confidence bounds are shown by the grey shaded boxes.

Correlations with south-westerly wave power at the western end were positive, but weak and lacked significance. In contrast, NAO showed a very strong negative correlation with easterly wave power at all locations along the full length of the coastline (Figure 7c). Conversely, WEPA showed a significant and positive correlation with total wave power (Figure 7e) and south-westerly wave power (Figure 7f) along the full length of the channel, with the strongest correlations and increased significance apparent at the western extent. There was no significant correlation between WEPA and easterly wave power at any node location (Figure 7g). The WDI was positively and significantly correlated with both NAO and WEPA along the full length of the coastline (Figure 7d,h).

3.2. Morphological Response to Wave Forcing

For all 22 sites analysed in this study, the BMR was calculated and is presented geographically in Figure 8. Sites with highly negative correlations such as Carlyon Bay (CAR), $R = -0.82$, Slapton Sands (SLP), $R = -0.86$ and Dawlish (DAW), $R = -0.87$ suggest that the beach response was highly rotational, with the two opposing beach ends responding out of phase with each other, likely attributable to

longshore sediment transport. At other locations, where BMR values were positive, for example Climping Harbour (CLI), $R = 0.78$, Praa Sands (PRA), $R = 0.50$, and Chesil Beach (CHE), $R = 0.85$, both ends of the beach appeared to be responding together, and the beach gained or lost volume as a single unit, suggesting transport was cross-shore dominated and spatially uniform across the beach length.

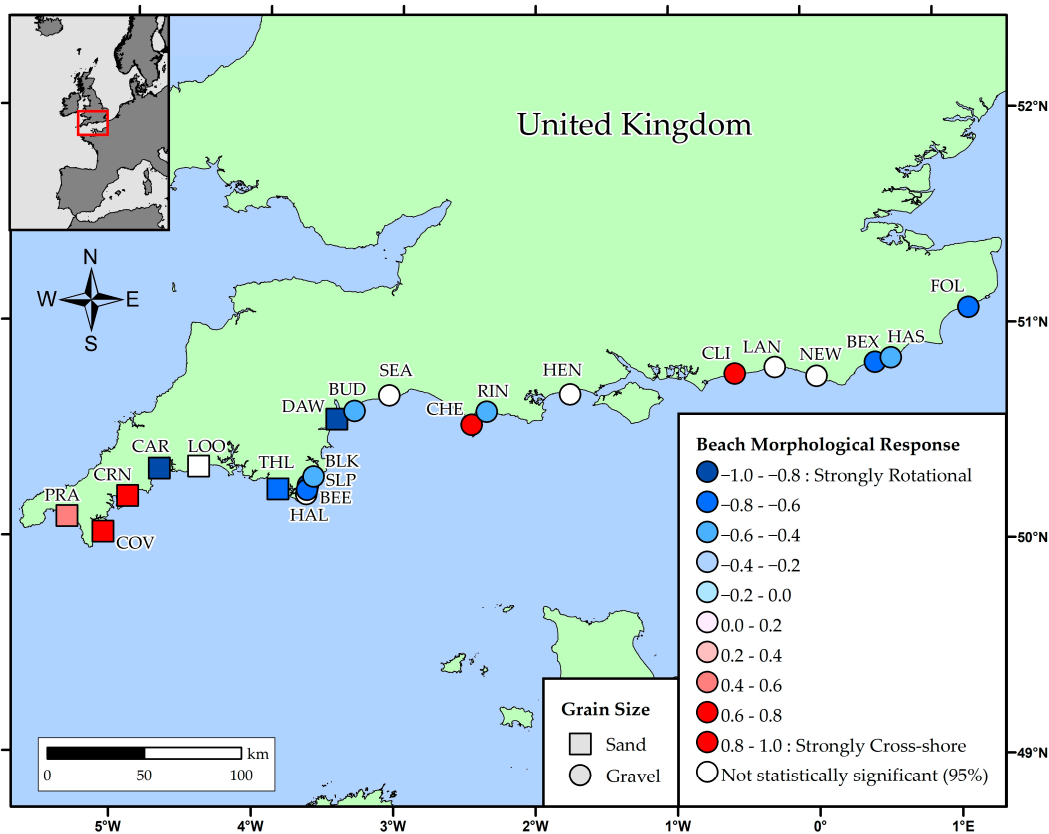


Figure 8. Beach morphological response at 22 coastal locations along the length of the south coast of England, U.K., calculated from multi-annual survey records. The strength and direction of the morphological response is indicated by the strength and colour of markers, with strongly-rotational (cross-shore) sites identified by dark blue (red) colours. White markers indicate sites in which the behavioural response is insignificant at the 95% confidence limit ($p > 0.05$). Square markers indicate sand sites, whilst circles indicate gravel beaches.

BMR values for each site are displayed relative to their average shore normal angle in Figure 9a, with the majority of sites that demonstrated significant negative (rotational) BMR values, orientated to face southeast, with average shore normal angles less than 180° . For sites with significantly positive (cross-shore) BMR values, beaches tended to face southwest (shore normal angles greater than 180°), towards the incoming dominant south-westerly waves. In addition, at all sites, for each time step of the survey record, the RI was linearly regressed against the WDI for the period between morphological surveys. The correlation between the two is presented in Figure 9b. Where correlations were positive, clockwise beach rotation occurred with increased positive values of the WDI, with dominance of south-westerly over easterly waves, and counter clockwise rotation occurred where there was a reversal in wave directional dominance. Where correlations were negative, the opposite was true, with counter clockwise rotation of the beach state under increased south-westerly waves. For all significant correlations, beach locations that exhibited clockwise rotation to increased WDI values were facing south east, with a shore normal angle that split the angle of the two bi-directional wave modes (south-westerly and easterly).

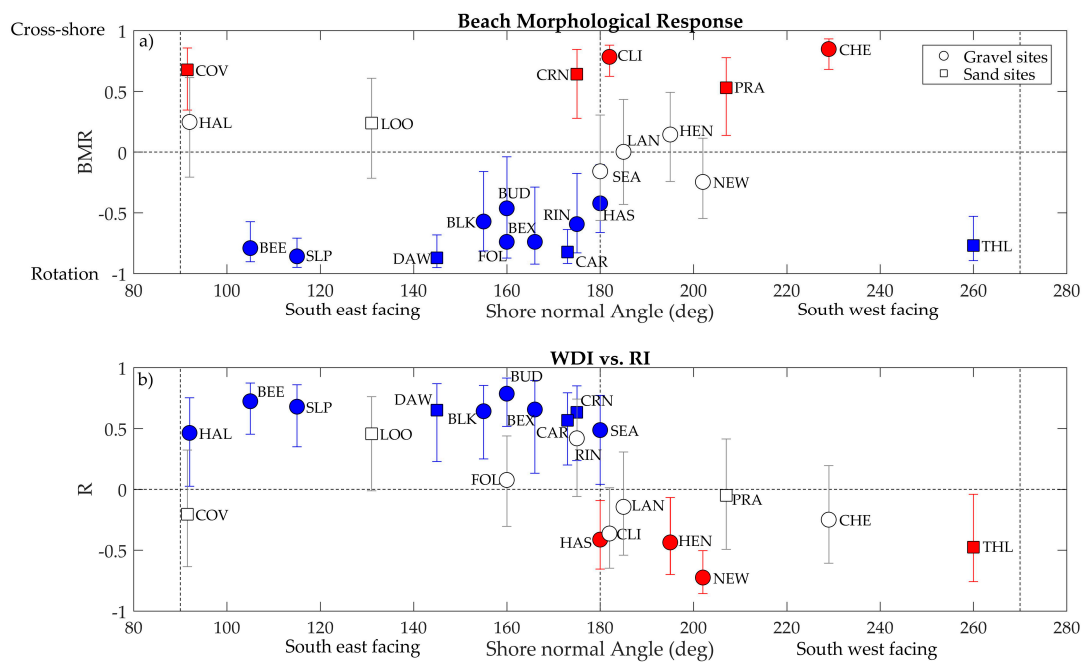


Figure 9. (a) Average shore-normal angle for each morphological site, plotted against its Beach Morphological Response (BMR) value. (b) The average shore-normal angle of coastline for each morphological site, plotted against the linear correlation coefficient (R) between the WDI and RI. Vertical dashed lines display the 90° and 180° shore-normal angles, with the areas in between representing south-easterly- and south-westerly-facing beaches. In both plots, gravel sites are denoted by circles, and sand sites by squares. Where site markers are white, correlation coefficients are not statistically significant at the 95% confidence limit ($p > 0.05$).

In addition to the shore normal angle, average beach slope (berm crest to MLWS) was calculated for each site and plotted against values of BMR (Figure 10). Sites with steeper slopes ($\tan\beta > 0.08$) displayed statistically-significant rotational values (negative BMR values). The majority of sites displaying cross-shore morphological responses (positive BMR values) had shallower slopes, with $\tan\beta < 0.08$ for all but one site, Chesil (CHE). Additionally, the majority of cross-shore responses were found at sand beaches, whereas rotational responses were more apparent at steeper, gravel beaches.

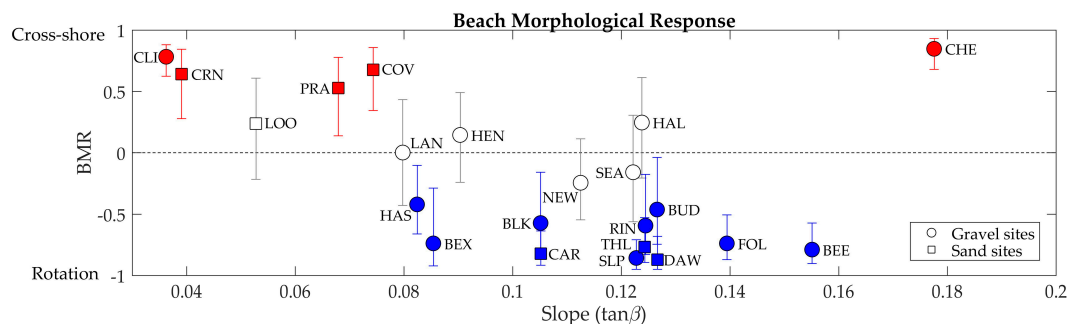


Figure 10. Average beach face slope ($\tan\beta$), plotted against its BMR value. Gravel sites are denoted by circles and sand sites by squares. Where site markers are white, correlation coefficients are not statistically significant at the 95% confidence limit ($p > 0.05$).

3.3. Atmospheric Control of Morphological Response

As shown previously, the WDI imparts strong controls on rotational beach behaviour at many of the south east-facing sites assessed in this study. Given the significant correlations of WDI with both NAO and WEPA, direct connections between atmospheric indices and beach rotation were

investigated. Slapton Sands (SLP), a long gravel barrier beach, and Carlyon Bay (CAR), a shorter, sandy embayed beach, both displayed strong rotational beach morphological responses over the duration of the study, and in both cases, RI was significantly correlated to WDI. Both sites had relatively complete morphological datasets, and the direct linear regression of RI against NAO and WEPA is displayed in Figure 11.

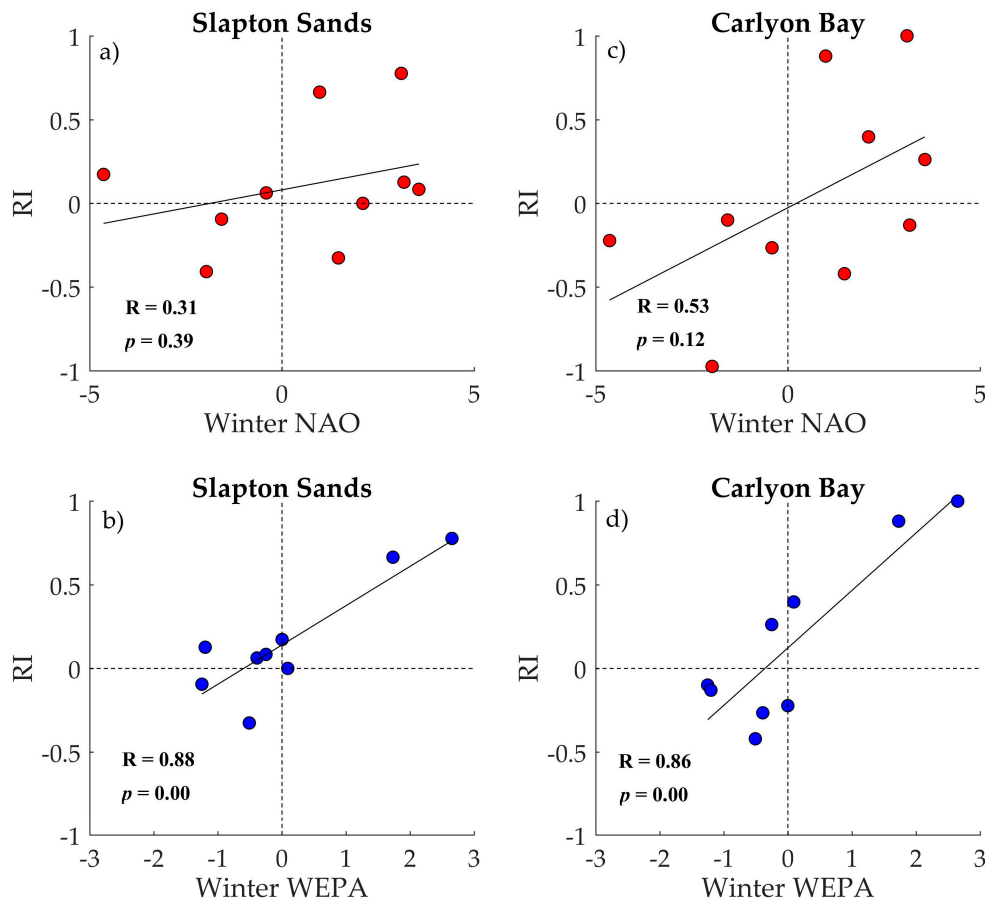


Figure 11. Direct correlations of the winter RI at Slapton Sands with winter values of (a) NAO and (b) WEPA. Additional correlations of winter RI at Carlyon Bay with winter values of (c) NAO and (d) WEPA.

Both sites displayed a weak positive correlation between the RI and NAO (Figure 11a,c); however, both were statistically insignificant ($p > 0.05$). In contrast, both sites displayed a strong, significant positive correlation (Figure 11b,d) between winter values of WEPA and the RI (Slapton Sands, $R = 0.88$; Carlyon Bay, $R = 0.86$). For both locations, the strongest positive (negative) RI values were associated with positive (negative) values of both NAO and WEPA, resulting in clockwise (anticlockwise) rotation.

4. Discussion

This study identified a bi-directional wave climate along the length of the English Channel, with dominant waves arriving from south-westerly directions and secondary modes coming from the east. Variability in the contribution of both modes of wave direction, and their relative balance over winter averaged seasons, has been shown to correlate well with the NAO and WEPA climate indices. Whilst winter wave height anomalies in the northern latitudes of the north east Atlantic Ocean were well correlated with both NAO and WEPA by Castelle et al. [13], Malagon Santos et al. [24] concluded that WEPA was better suited to predicting increased wave height in the south west region; however, directionality was not taken into account, and the results of the present study show that

wave bi-directionality is also linked to NAO and WEPA, along the entirety of the English Channel. Easterly wave power contributions were well correlated to negative phases of the winter NAO, whilst high contributions of south-westerly waves were correlated with positive values of winter WEPA. Both indices had some spatial variability in their influence on wave conditions along the coastline, with WEPA imparting a stronger control in the western extent of the channel, whilst NAO was shown to have stronger, more significant correlations in the eastern reaches.

Previous site-specific evidence of beach rotation at an embayed series of interlinked gravel barriers by Wiggins et al. [4] suggested that the WDI could be used to predict along-shore changes in beach morphology at similar semi-sheltered sites over different timescales. Within this study, several beach sites had been identified that displayed rotational behaviour, with beach extremities responding out of phase with each other. It must be noted that only inter-tidal beach volumes have been assessed within this study, and in some cases, rotational signals may be weakened or obscured due to exchanges occurring from the inter-tidal to sub-tidal domain. In almost all significant cases, beach rotation appeared to be linked with shoreline alignment, with coastlines oriented towards the south east, experiencing the most oblique incident waves under dominant south-westerly conditions, driving clockwise beach rotation, whilst counter rotating under easterly waves.

Where sites faced south west, towards the angle of dominant south-westerly wave approach, significant cross-shore morphological responses were observed, with both ends of the beach gaining or losing volume at the same time. This response is likely attributable to increased exposure to south-westerly waves and perhaps increased shelter, and reduced influence, from easterly waves. Burvingt et al. [25] observed a similar result, identifying a strong relationship between shoreline orientation and beach rotation, at a multitude of south-easterly-facing beaches following an exceptionally energetic winter season, dominated by south-westerly storm events [26–28]. Despite their observations only spanning a single winter season, rotational behaviour was consistent within the western beaches of the English Channel and was furthermore correlated to normalised beach length (not assessed in this study), with longer, narrower beaches experiencing greater levels of rotation. Additionally, the studies conducted by Burvingt et al. [25] and Scott et al. [28] both identified the same cross-shore response at south west-facing beaches, where dominant storm waves approached from a shore-normal angle, although the wave climate at these locations under the observed winter period was unidirectional. Within the present study, beach slope and sediment type were also found to impart some control on the observed morphological responses (Figure 10). Steeper, predominantly gravel beaches, exhibited rotational behaviour, and shallower, sandier beaches displayed a cross-shore response; however, quantitative assessment of beach grain size was not conducted here.

Where rotational behaviour was identified in this study, the RI at each site was well correlated with the WDI, especially for south east-facing beaches, implying that the magnitude and direction (clockwise/counter-clockwise) of beach rotation is controlled by the balance of south-westerly to easterly wave power. This agrees with the findings of Wiggins et al. [4], which presented evidence of clockwise and counter-clockwise rotation under south-westerly and easterly winters, respectively. Similar results of beach rotation at the same location were presented by Ruiz de Alegria-Arzaburu and Masselink [9], for contrasting storm events from opposing directions. Although their results showed agreement with the current study, in that the balance of contrasting wave directions controls the rotational beach state, they also noted that storm-induced sediment transport rates may be asymmetrical between the two wave directions, given the shoreline angle and differing wave types. This may also explain why there are some anomalous results within the regional assessment. For example, both Coverack beach (COV) and Hallsands (HAL) displayed a cross-shore BMR response (Figure 9a), despite being the most easterly facing beaches in the analysis. At both locations, shelter from south-westerly waves is provided by proximity to prominent headlands, meaning exposure to oblique south westerlies may be limited, and approaching easterly waves are shore-normal. Additionally, both beaches are very short in length, which is less conducive to rotation as suggested by Burvingt et al. [2,25]. Additionally, the morphometric parameters of headland geometry in relation to the incoming wave climate can lead to

wave shadowing from different directions, inducing gradients in alongshore wave energy. In some cases, this can result in beach rotation as a function of variable cross-shore exchanges at different alongshore locations [15,29], rather than directly due to changes in dominant wave direction.

Due to the strong correlations between atmospheric indices and wave climate, in addition to the significant link between WDI and RI, beach rotation may potentially be inferred from atmospheric indices, perhaps allowing wave climate to be omitted when assessing coastline vulnerability to erosive rotational events. For the majority of sites in this study, RI was not significantly well correlated with either winter NAO or winter WEPA, at the timescales assessed here. This is potentially due to the limited temporal dataset, restricting available data points to no more than 10 years; however, both Slapton Sands and Carlyon Bay did show strong BMR values (Figure 9a), correlations between RI and WDI (Figure 9b), and a statistically-significant positive correlation between RI and winter WEPA (Figure 11b,d). This consistency within the analysis suggests that positive (negative) rotation may be predicted at each site with positive (negative) winter forecasts of WEPA.

Despite both sites showing statistically insignificant correlations between RI and winter NAO, the index should not be ignored. For the southeast-facing beaches, it is likely that strong negative NAO winters result in increased easterly wave events, reducing the extent of winter-induced clockwise rotation, as a result of south-westerly waves. Conversely, when both the NAO and WEPA are in phase, it is likely that the combined influence of the two indices may amplify the effects of rotation, whether clockwise or anticlockwise. This is apparent from the synchronous high values of the NAO and WEPA during the winter of 2013/2014, recently described as the most energetic since at least 1953 [26–28]. During that winter, significant clockwise rotation was observed at many south coast locations, leaving coastal communities and infrastructure at risk from future storm events. Both Slapton Sands and Carlyon Bay experienced their largest rotation in the 10-year survey record during the 2013/2014 winter, well described by high values of both WEPA and NAO (Figure 11), despite Castelle et al. [13] identifying that NAO and WEPA indices were not correlated. The combination of high values for both indices within the same winter led to higher than average wave heights in the North Atlantic [13] and storms tracking more southerly than usual [27]. Similar signals of enhanced beach rotation have been observed under several winters with increased El Niño (negative ENSO) along the coast of the Pacific North West [30]. Many dissipative sandy beaches were observed to rotate anti-clockwise (northwards) under large storm waves approaching from increased southerly directions [31]; however, their findings were somewhat different from those found here, as the current study identified opposing wave directions under climate variability, rather than subtle shifts in average wave angle and storm wave height.

In many cases, associated recovery (reversals in direction) of beach rotational events can take several years [28], particularly if sediment is transported out of littoral cells around headlands [4,28,32] and directional longshore transport is asymmetrical [9]. A key example is the embayment scale rotation observed in Start Bay following the winter of 2013/2014, where 294,000 m³ of gravel were recorded as bypassing significant headlands, leaving littoral sub-cells depleted of volume. As of 2018, measurements have shown that despite some reversals in wave directions [4], the material has yet to return to its original cell, and the embayment continues to maintain its decadal-scale rotation northwards.

Despite this study showing that climate indices have a regional impact on wave climate, combinations of multiple indices may be required for direct predictions of rotational beach behaviour across larger spatial scales. At site-specific locations, where increased beach rotation poses a risk to sea defences, tourist infrastructure, roads and ecological and environmental assets, even qualitative predictions of rotational direction, or timescales of recovery, derived from forecast climate indices would be a welcome addition to the tools available to coastal managers.

Recent improvements to seasonal forecasts of winter NAO [20,21,33] mean that year-ahead estimates of beach response may be possible, especially for regions similar to this study, where many sites are identified as having a highly-rotational BMR. This would allow coastal managers and

engineers to prepare for potential winter rotational impacts, taking a pro-active approach to either soft engineering works (e.g., beach recycling/recharge) or hard coastal defences.

5. Conclusions

Strong bi-directionality of the winter wave climate along the south coast of England was identified at 14 model node locations, with south-westerly waves dominant over easterly waves. The winter averaged atmospheric indices of NAO and WEPA were strongly negatively and positively correlated with easterly and south-westerly waves, respectively.

The morphological response of 22 beach locations was assessed over a decadal timescale (winter seasons). Eleven of these sites displayed a statistically-significant rotational beach morphological response, with rotation being strongest at south east-facing beaches, attributed to increased obliquity to both the south-westerly and easterly wave directions. A cross-shore response was identified at south west-facing beaches, with limited rotation observed as beaches tend towards the dominant direction of wave approach.

Of the rotating beaches, eight of the 11 were gravel beaches, and all had relatively steep beach faces ($\tan\beta > 0.08$). Cross-shore beach responses were more prominent in sandy beaches with shallow beach face slopes ($\tan\beta < 0.08$).

The rotation index, calculated from morphological beach volume change, and an index of the balance of directional wave power were significantly positively correlated with each other at the majority of south east-facing, rotational sites.

Author Contributions: Conceptualization, M.W., T.S. and G.M.; methodology, M.W., T.S. and G.M.; formal analysis, M.W. and T.S.; investigation, M.W. and T.S.; resources, M.W.; data curation, M.W.; writing, original draft preparation, M.W.; writing, review and editing, M.W., T.S., G.M., P.R. and N.V.; visualization, M.W. and N.V.; supervision, T.S., G.M. and P.R.; project administration, G.M.; funding acquisition, G.M.

Funding: This research was funded by the U.K. Natural Environment Research Council, Grant Number NE/M004996/1; BLUE-coast project. The APC was funded by the University of Plymouth.

Acknowledgments: The authors would like to thank the United Kingdom Meteorological Office, The Climate Data Guide, Bruno Castelle, Plymouth Coastal Observatory and the Channel Coastal Observatory.

Conflicts of Interest: The authors declare no conflict of interest.

Appendix A

Table A1. Morphological survey site code, with local name, U.K. county, coordinates, beach length, sediment type and average beach slope.

Code	Name	County	Coordinates	Length (km)	Sediment	Slope ($\tan\beta$)
PRA	Praa Sands	Cornwall	50.1045° N, 5.3857° W	1.6	Sand	0.07
COV	Coverack	Cornwall	50.0244° N, 5.0976° W	0.5	Sand	0.07
CRN	Carne	Cornwall	50.2071° N, 4.9380° W	1.2	Sand	0.04
CAR	Carlyon Bay	Cornwall	50.3370° N, 4.7467° W	1.3	Sand	0.11
LOO	Looe Beach	Cornwall	50.3522° N, 4.4522° W	0.3	Sand	0.05
THL	Thurlestone	Devon	50.2655° N, 3.8541° W	0.6	Sand	0.12
HAL	Hallsands	Devon	50.2361° N, 3.6597° W	0.2	Gravel	0.12
BEE	Beesands	Devon	50.2532° N, 3.6575° W	1.4	Gravel	0.16
SLP	Slapton Sands	Devon	50.2833° N, 3.6333° W	5.2	Gravel	0.12
BLK	Blackpool Sands	Devon	50.3194° N, 3.6102° W	0.7	Gravel	0.11
DAW	Dawlish Town	Devon	50.5809° N, 3.4640° W	1.0	Sand	0.13
BUD	Budleigh	Devon	50.6310° N, 3.3202° W	3.1	Gravel	0.13
SEA	Seaton	Devon	50.7053° N, 3.0719° W	2.1	Gravel	0.12
CHE	Chesil Beach	Dorset	50.6267° N, 2.5605° W	4.1	Gravel	0.18
RIN	Ringstead	Dorset	50.6309° N, 2.3512° W	0.5	Gravel	0.12
HEN	Hengistbury	Dorset	50.7191° N, 1.7661° W	1.4	Gravel	0.09
CLI	Climping	W Sussex	50.7978° N, 0.5734° W	1.8	Gravel	0.04
LAN	Lancing	W Sussex	50.8282° N, 0.3281° W	1.8	Gravel	0.08
NEW	Newhaven	E Sussex	50.7931° N, 0.0456° E	1.0	Gravel	0.11
BEX	Bexhill	E Sussex	50.8499° N, 0.4662° E	1.0	Gravel	0.09
HAS	Hastings	E Sussex	50.8543° N, 0.5735° E	1.0	Gravel	0.08
FOL	Folkestone	Kent	51.0737° N, 1.1703° E	0.9	Gravel	0.14

Table A2. Morphological survey site code, with local name, total number of surveys, start year of survey programme and frequency.

Code	Name	Surveys	Start Year	Frequency
PRA	Praa Sands	25	2007	6 monthly
COV	Coverack	22	2007	6 monthly
CRN	Carne	21	2007	6 monthly
CAR	Carlyon Bay	27	2007	6 monthly
LOO	Looe Beach	22	2007	6 monthly
THL	Thurlestone	25	2007	6 monthly
HAL	Hallsands	22	2007	4/6 monthly
BEE	Beesands	26	2007	4/6 monthly
SLP	Slapton Sands	25	2007	4/6 monthly
BLK	Blackpool Sands	20	2007	6 monthly
DAW	Dawlish Town	23	2007	6 monthly
BUD	Budleigh	22	2007	6 monthly
SEA	Seaton	21	2007	6 monthly
CHE	Chesil Beach	30	2007	4/6 monthly
RIN	Ringstead	19	2007	6 monthly
HEN	Hengistbury	29	2005	6 monthly
CLI	Climping	31	2007	4/6 monthly
LAN	Lancing	28	2007	4 monthly
NEW	Newhaven	33	2007	4 monthly
BEX	Bexhill	38	2003	4 monthly
HAS	Hastings	38	2003	4 monthly
FOL	Folkestone	34	2003	4 monthly

References

1. Klein, A.H.D.F.; Filho, L.B.; Schumacher, D.H. Short-Term Beach Rotation Processes in Distinct Headland Bay Beach Systems. *J. Coast. Res.* **2002**, *18*, 442–458.
2. Burvingt, O.; Masselink, G.; Russell, P.; Scott, T. Classification of beach response to extreme storms. *Geomorphology* **2017**, *295*, 722–737. [[CrossRef](#)]
3. Bergillos, R.J.; Masselink, G.; Ortega-Sánchez, M. Coupling cross-shore and longshore sediment transport to model storm response along a mixed sand-gravel coast under varying wave directions. *Coast. Eng.* **2017**, *129*, 93–104. [[CrossRef](#)]
4. Wiggins, M.; Scott, T.; Masselink, G.; Russell, P.; Mccarroll, R.J. Coastal embayment rotation: Response to extreme events and climate control, using full embayment surveys. *Geomorphology* **2019**, *327*, 385–403. [[CrossRef](#)]
5. Thomas, T.; Phillips, M.R.; Williams, T.A. A Centurial Record of Beach Rotation. *J. Coast. Res.* **2013**, 594–599. [[CrossRef](#)]
6. Nicholls, R.J.; Marinova, N.; Lowe, J.A.; Brown, S.; Vellinga, P.; de Gusmao, D.; Hinkel, J.; Tol, R.S.J. Sea-level rise and its possible impacts given a “beyond 4°C world” in the twenty-first century. *Philos. Trans. R. Soc. A Math. Phys. Eng. Sci.* **2011**, *369*, 161–181. [[CrossRef](#)]
7. Suursaar, Ü.; Jaagus, J.; Tõnisson, H. How to quantify long-term changes in coastal sea storminess? *Estuar. Coast. Shelf Sci.* **2015**, *156*, 31–41. [[CrossRef](#)]
8. Pontee, N. Defining coastal squeeze: A discussion. *Ocean Coast. Manag.* **2013**, *84*, 204–207. [[CrossRef](#)]
9. Ruiz de Alegria-Arzaburu, A.; Masselink, G. Storm response and beach rotation on a gravel beach, Slapton Sands, U.K. *Mar. Geol.* **2010**, *278*, 77–99. [[CrossRef](#)]
10. Wiggins, M.A.; Scott, T.; Masselink, G.; Russell, P.; Castelle, B.; Dodet, G. The role of multi-decadal climate variability in controlling coastal dynamics: re-interpretation of the “Lost Village of Hallsands.”. In Proceedings of the Proceedings Coastal Dynamics 2017, Helsingor, Denmark, 12–16 June 2017; pp. 96–107.

11. Dolphin, T.J.; Vincent, C.E.; Wihsgott, J.; Belhache, M.; Bryan, K.R. Seasonal rotation of a mixed sand-gravel beach. *J. Coast. Res.* **2011**, *SI64*, 65–69.
12. Thomas, T.; Phillips, M.R.; Williams, A.T.; Jenkins, R.E. Medium timescale beach rotation; gale climate and offshore island influences. *Geomorphology* **2011**, *135*, 97–107. [[CrossRef](#)]
13. Castelle, B.; Dodet, G.; Dodet, G.; Scott, T. A new climate index controlling winter wave activity along the Atlantic coast of Europe: the West Europe Pressure Anomaly. *Geophys. Res. Lett.* **2017**, *44*, 1384–1392. [[CrossRef](#)]
14. Ranasinghe, R.; McLoughlin, R.; Short, A.; Symonds, G. The Southern Oscillation Index, wave climate, and beach rotation. *Mar. Geol.* **2004**, *204*, 273–287. [[CrossRef](#)]
15. Harley, M.D.; Turner, I.L.; Short, A.D. New insights into embayed beach rotation: The importance of wave exposure and cross-shore processes. *J. Geophys. Res. Earth Surf.* **2015**, 1–15. [[CrossRef](#)]
16. Barnard, P.L.; Short, A.D.; Harley, M.D.; Splinter, K.D.; Vitousek, S.; Turner, I.L.; Allan, J.; Banno, M.; Bryan, K.R.; Doria, A.; et al. Coastal vulnerability across the Pacific dominated by El Niño/Southern Oscillation. *Nat. Geosci.* **2015**, *8*, 801. [[CrossRef](#)]
17. Masselink, G.; Austin, M.; Scott, T.; Poate, T.; Russell, P. Role of wave forcing, storms and NAO in outer bar dynamics on a high-energy, macro-tidal beach. *Geomorphology* **2014**, *226*, 76–93. [[CrossRef](#)]
18. Autret, R.; Dodet, G.; Suanez, S.; Roudaut, G.; Fichaut, B. Long-term variability of supratidal coastal boulder activation in Brittany (France). *Geomorphology* **2017**, *304*, 184–200. [[CrossRef](#)]
19. Burvingt, O.; Masselink, G.; Scott, T.; Davidson, M.; Russell, P. Climate forcing of regionally-coherent extreme storm impact and recovery on embayed beaches. *Mar. Geol.* **2018**, *401*, 112–128. [[CrossRef](#)]
20. Scaife, A.; Yu Karpechko, A.; Baldwin, M.; Brookshaw, A.; Butler, A.; Eade, R.; Gordon, M.; Maclachlan, C.; Martin, N.; Dunstone, N.; et al. Seasonal winter forecasts and the stratosphere. *Atmos. Sci. Lett.* **2015**, *17*, 51–56. [[CrossRef](#)]
21. Dunstone, N.; Smith, D.; Scaife, A.; Hermanson, L.; Eade, R.; Robinson, N.; Andrews, M.; Knight, J. Skilful predictions of the winter North Atlantic Oscillation one year ahead. *Nat. Geosci.* **2016**, *9*, 809. [[CrossRef](#)]
22. Castelle, B.; Dodet, G.; Masselink, G.; Scott, T. Increased Winter-Mean Wave Height, Variability, and Periodicity in the Northeast Atlantic Over 1949–2017. *Geophys. Res. Lett.* **2018**, *45*, 3586–3596. [[CrossRef](#)]
23. Hurrell, J.W.; National Center for Atmospheric Research Staf (Eds.) “The Climate Data Guide: Hurrell North Atlantic Oscillation (NAO) Index (station-based)”. Available online: <https://climatedataguide.ucar.edu/climate-data/hurrell-north-atlantic-oscillation-nao-index-station-based> (accessed on 4 August 2018).
24. Malagon Santos, V.; Haigh, I.; Wahl, T. Spatial and Temporal Clustering Analysis of Extreme Wave Events around the U.K. Coastline. *J. Mar. Sci. Eng.* **2017**, *5*, 28. [[CrossRef](#)]
25. Burvingt, O.; Masselink, G.; Russell, P.; Scott, T. Beach response to consecutive extreme storms using LiDAR along the SW coast of England. *J. Coast. Res.* **2016**, 1052–1056. [[CrossRef](#)]
26. Masselink, G.; Scott, T.; Poate, T.; Russell, P.; Davidson, M.; Conley, D. The extreme 2013/2014 winter storms: hydrodynamic forcing and coastal response along the southwest coast of England. *Earth Surf. Process. Landforms* **2015**, *41*, 378–391. [[CrossRef](#)]
27. Masselink, G.; Castelle, B.; Scott, T.; Dodet, G.; Suanez, S.; Jackson, D.; Floc’H, F. Extreme wave activity during 2013/2014 winter and morphological impacts along the Atlantic coast of Europe. *Geophys. Res. Lett.* **2016**, *43*, 2135–2143. [[CrossRef](#)]
28. Scott, T.; Masselink, G.; Hare, T.O.; Saulter, A.; Poate, T.; Russell, P.; Davidson, M.; Conley, D. The extreme 2013 / 2014 winter storms: Beach recovery along the southwest coast of England. *Mar. Geol.* **2016**, *382*, 224–241. [[CrossRef](#)]
29. Harley, M.D.; Turner, I.L.; Short, A.D.; Ranasinghe, R. A reevaluation of coastal embayment rotation: The dominance of cross-shore versus alongshore sediment transport processes, Collaroy-Narrabeen Beach, southeast Australia. *J. Geophys. Res. Earth Surf.* **2011**, *116*, 1–16. [[CrossRef](#)]
30. Peterson, C.D.; Jackson, P.L.; O’Neil, D.J.; Rosenfeld, C.L.; Kimerling, A.J. Littoral Cell Response to Interannual Climatic Forcing 1983–1987 on the Central Oregon Coast, USA. *J. Coast. Res.* **1990**, *6*, 87–110.
31. Anderson, D.; Ruggiero, P.; Antolínez, J.A.A.; Méndez, F.J.; Allan, J. A Climate Index Optimized for Longshore Sediment Transport Reveals Interannual and Multidecadal Littoral Cell Rotations. *J. Geophys. Res. Earth Surf.* **2018**, *123*, 1958–1981. [[CrossRef](#)]

32. Valiente, N.G.; McCarroll, R.J.; Masselink, G.; Scott, T.; Conley, D. Role of waves and tides on depth of closure and potential for headland bypassing. *Mar. Geol.* **2018**, *407*, 60–75. [[CrossRef](#)]
33. Wang, L.; Ting, M.; Kushner, P.J. A robust empirical seasonal prediction of winter NAO and surface climate. *Sci. Rep.* **2017**, *7*, 279. [[CrossRef](#)]



© 2019 by the authors. Licensee MDPI, Basel, Switzerland. This article is an open access article distributed under the terms and conditions of the Creative Commons Attribution (CC BY) license (<http://creativecommons.org/licenses/by/4.0/>).